Preparation of effective lithium-ion sieve from sludge-generated TiO_2

Sayed Mukit Hossain [1], Idris Ibrahim [1], Youngwoo Choo [1], Amir Razmjou [1], Gayathri Naidu [1], Leonard Tijing [1], Jong-Ho Kim [2], and Ho Kyong Shon [1, *]

[1] Faculty of Engineering and IT, University of Technology, Sydney, P.O. Box 123, Broadway, NSW 2007, Australia; sayed.m.hossain@student.uts.edu.au (S.M.H.); Idris.ibrahim@student.uts.edu.au (I.I.); youngwoo.choo@uts.edu.au (Y.C.); amir.razmjouchaharmahali@uts.edu.au (A.R.C.); gayathri.danasamy@uts.edu.au (G.N.); leonard.tijing@uts.edu.au (L.T.); Hokyong.Shon-1@uts.edu.au (H.K.S.)

[2] School of Chemical Engineering, Chonnam National University, 77 Yongbong-ro, Buck-gu, Gwangju 61186, Korea; jonghkim@jnu.ac.kr (J.-H.K)

*Correspondence: Hokyong.Shon-1@uts.edu.au (H.K.S.); Tel.: +61 447 332 707 (H.K.S.)

Abstract

A potential adsorbent for Li^+ extraction from liquid resources is titanium-type lithium-ion sieves (LISs) because of their structural stability and high adsorption capacity. However, the adsorption efficiency and recycling stability of LISs produced with various TiO_2 precursors vary significantly. Additionally, traditional TiO_2 is often produced using chemical-intensive methods, resulting in large amounts of effluent containing strong acids and high concentrations of chloride/sulfate ions, posing a threat to the environment. Hence, in this study, the LIS precursors, Li_2TiO_3, were synthesized utilizing novel environment-friendly anatase titania made from flocculated sludges of synthetic secondary sewage effluent (S-LTO) and dye wastewater (D-LTO). The physicochemical characteristics and adsorption capacities of the synthesized LISs were then investigated. The results indicated that sludge-generated LISs could be effectively produced and had a high Li^+ adsorption capacity of 35.43 mg/g for S-LTO and 34.97 mg/g for D-LTO. For the synthesized LISs, the adsorption kinetics and isotherms verified a fixed energy-based monolayer chemisorption. Furthermore, the H_2TiO_3 generated from sludge was extremely stable after acid pickling, reusable (4 regeneration cycles exhibited minimal performance degradation), and highly selective to Li^+ in an aqueous medium, suggesting enormous industrial potentials such as seawater and brine for aqueous Li^+ recovery.

Key words: Lithium, Adsorption, Brine, Sludge-generated TiO_2, Lithium ion Sieve.

1 Introduction

Lithium (Li) is one of the most valuable metals, with many industrial uses and rising market demand. For instance, by 2100, the demand for Li is projected to grow from 45.0 kt to 1.0 Mt, a tenfold increase [1]. Because of the rapid development of the market, Li has been widely used in a variety of industries, including the metallurgical, pharmaceutical, and Li secondary battery industries [1-5]. Studies have shown that to run a single fusion reactor for a year, 787 ton of Li are needed [6, 7]. Accelerated expansion in the Li-battery sector, on the other hand, has increased its annual growth by 8.9% in 2019 [3]. Due to the increasing Li market, scientists are focusing on Li recovery from various sources, including salt lakes, brines, mines, seawater, spodumene, and amblygonite [5, 6, 8-10]. Conventionally, the majority of Li is mined from mineral ores such as spodumene and brines [9, 11-13]. However, Li extraction from mineral ore deposits typically requires a higher energy input (~ 200 MJ/kg) and has a more significant environmental impact than Li extraction from brines, which requires a lower energy input (~ 80 MJ/kg) with minimal environmental impact [1, 14, 15]. Thus, by 2050, it is anticipated to be heavily-reliant on low-grade Li sources (Li^+ < 100 mg/L, Mg^{2+}/Li^+ > 10) [1, 10]. Besides, around a quarter of the potential Li supply resides in brines with low Li content [16]. Furthermore, since seawater has a relatively low Li content (~ 0.15 mg/L), Li recovery from seawater is not considered adequate to fulfill Li needs [3]. As a consequence, scientists have begun to investigate novel sources and methods for extracting Li from aqueous medium.

Traditionally, Li has been recovered from high-grade brines using solar evaporation followed by a precipitation method [3, 17]. However, evaporation may take years to produce the required Li concentration, depending on the brine quality [12]. Moreover, the evaporation-precipitation approach is not appropriate for low-grade brines owing to the simultaneous settling of magnesium [3, 18]. Because of the limitations of conventional evaporation-precipitation schemes, solvent extraction [5, 19, 20], electrodialysis [21, 22], electrochemical ion pumping [18, 23], and selective adsorption [2, 3, 24, 25] of Li ions from brines are gaining popularity. Because of their selectivity for Li, Li chelating extractants like 14-crown-4-ethers are the most researched [26]. On the other hand, solvent extraction

has a number of drawbacks (e.g., expensive crown ethers, brine science) and is used in just a few industrial settings [1]. Furthermore, in low-grade brine, electrochemical ion extraction and electrodialysis are more energy-intensive compared to adsorption [27]. Therefore, adsorption is one of the most attractive processes owing to its simplicity, ability to give results quickly compared to conventional evaporative techniques, and low cost of implementation [6, 11, 17, 28]. Ionic sieve substances, viz., delithiated hydrogen manganese oxides (HMOs) [9, 29] and hydrogen titanium oxides (HTOs) [4, 25], have demonstrated high selectivity for aqueous Li recovery. These adsorbents allow Li ions to be inserted and removed without generating substantial crystalline disruption. Na^+, K^+, and Ca^{2+} are some of the main ions found in brine that are not capable of adsorbing to the surface of the adsorbent owing to their bigger atomic radius [24, 30, 31]. Additionally, the significant hydration energy of Mg^{2+} limits Mg^{2+} to adsorb on HMOs/HTOs [31]. The spinel-structured $LiMn_2O_4$ [13, 20, 32], $Li_{1.33}Mn_{1.67}O_4$ [33], $Li_{1.6}Mn_{1.6}O_4$ [34], $Li_{1.5}Mn_2O_4$ [3] and $Li_4Mn_5O_{12}$ [35, 36] have been demonstrated to be helpful for selective Li recovery from aqueous solutions. However, the dissolution of Mn from the LMO matrix happens during the elution of Li from the matrix in dilute acidic solutions, which results in decreased adsorption potential and poor reusability [6, 17, 20, 25].

Much like Mn-based spinel oxides, Ti-based spinel oxides offer many of the same advantages. Furthermore, since Ti is a plentiful resource on the planet, it is more environmentally benign than other metals, and unlike HMOs, it does not dissolute in mild acid [37]. HTO has been identified as a potential environmentally friendly sorbent to extract lithium from brine [24, 30, 31]. Nanosized Li_2TiO_3 [31, 38-40] and $Li_4Ti_5O_{12}$ [41] have demonstrated greater endurance when recovering Li. The oxygen atoms in Li_2TiO_3 are packed in cubic closed packing in the crystal system, while Li and Ti fill the octahedral voids, creating a layered monoclinic structure [1, 3]. In the layered monoclinic structure, one layer comprises Li atoms, while the other layer has the $LiTi_2$ chain. LTOs are recyclable because of their strong structural integrity during lithium adsorption and desorption [25]. At a pH greater than 7, layered HTO undergoes ion exchange with Li ions in an aqueous solution containing Li ions to produce Li_2TiO_3. Later, through treating Li_2TiO_3 with HCl solution, Li can be retrieved. H_2TiO_3 has a theoretical ion exchange capacity of up to 143 mg/g [42], although the highest actual ion exchange capability to date

82 is 94.5 mg/g [28]. Because only 75% of the hydrogen-filled ion exchange sites in H_2TiO_3 can be
83 exchanged for Li^+, this is the maximum potential possible [43]. The isotherm of H_2TiO_3 showed
84 Langmuir-like behavior, as predicted by the pseudo-second-order rate model [31, 39]. The ion exchange
85 potential of H_2TiO_3 improves when Li^+ concentration and the pH of the aqueous solution increase [3].
86 Research showed the ion exchange potential of H_2TiO_3 rose from 12.0 to 32.0 mg/g when the starting
87 concentration of Li^+ was increased from 500 to 2500 mg/L at pH higher than 12.50 [25]. To better
88 understand the factors influencing the ion exchange potential of H_2TiO_3, a systematic orthogonal test
89 was performed using a variety of variables, including pre-calcination temperature, Li:Ti molar ratio,
90 calcination temperature, ion exchange temperature, and Li^+ concentration. The maximum ion exchange
91 potential of 57.8 mg/g was obtained under optimal conditions [44]. To make H_2TiO_3 more cost-effective,
92 low-grade titanium slag was utilized as the starting material, and the optimum capacity was 27.8 mg/g
93 [38].

94 In most studies concerning HTOs, commercial titania is processed with Li salts, and either solid-
95 state synthesis or wet chemistry is used to synthesize LTOs [45]. However, TiO_2 is often made via
96 chemical-intensive techniques, with chloride, sulfate, and alkoxide being typical ingredients. The
97 problem with these techniques is that they produce large quantities of wastewater, which include strong
98 acids and high concentrations of chloride/sulfate ions, which are harmful to the environment. As a result,
99 a more environmentally friendly and sustainable TiO_2 manufacturing technique is required. On the other
100 hand, the production of perilous sludge resulting from wastewater treatment trains (primarily
101 flocculation/coagulation) is also seen as a severe problem of the water industry [46]. Traditionally, Al
102 and Fe-based salts in different forms have been utilized as efficient coagulants. However, the usage of
103 these traditional coagulants comes with inevitable environmental and financial consequences. These
104 constraints include: a) the subsequent processing of a large volume of created sludge, b) the effects of
105 residual trace metals in treated water, and c) small floc size and lengthy settling time [46-49]. As a
106 result, researchers are constantly exploring novel forms of coagulants to address these limitations.
107 Following that endeavor, Shon, Vigneswaran, Kim, Cho, Kim, Kim and Kim [49] reported the use of
108 $TiCl_4$ as a coagulant option for wastewater treatment. Since then, the low toxicity of Ti metal [50] and

the possibility of titania recovery [51-53] during Ti-based coagulation have piqued scientists' interest. In addition, the developed Ti-based salts in the last two decades have shown performance results at par with those of the conventional coagulants. Table S1 illustrates a comparison of the key findings of Ti-based coagulation and coagulation associated with conventional coagulants.

Handling excess sludge would cost between 25% to 65% of the overall cost of wastewater treatment facilities [51]. The successful reuse of treated wastewater, by-products, and residues generated during the treatment phase enabled the idea of wastewater treatment for the preservation of the environment and valuable resources [51, 54, 55]. TiO_2 is produced when sludge-generated by Ti^{4+} salt-based flocculation of wastewater is calcined [47, 49, 56]. The proposed sludge recycling method showed a lot of promise in lowering sludge disposal costs while still generating a useful by-product from sludge calcination. To determine the economic feasibility of using $TiCl_4$ to remove phosphorus from wastewater and synthesize photocatalyst grade TiO_2, Gong, Joo and Kim [57] conducted an economic study; where, in a water treatment facility with a capacity of 330,000 m^3/d, the prices of $TiCl_4$ and PAC for sewage treatment were compared. They have reported that it is possible to recover about 1 ton of TiO_2 from the coagulation sludge produced by 12 tons of $TiCl_4$ in a batch process. Taking into account the impurity of recovered TiO_2 from coagulation sludge, the selling price of the obtained TiO_2 was adjusted to be ten times less ($4.5/kg) than the selling price of P25 (Degussa), as shown in Table S2 and S3. Nonetheless, the synthesis of TiO_2 from Ti coagulation sludge might offset the high cost of $TiCl_4$ and provide extra profits ($3017/day) compared to PAC. Additionally, the production of TiO_2 from sludge, on the other hand, would substantially decrease the quantity of acidic waste generated during the sulfate and chlorine production scheme of titania [58].

Hence, this study developed a Li-ion sieve from sludge-generated titania through a facile solid-state reaction. We have used sludge-generated titania from synthetic secondary sewage effluent and dye wastewater treatment plant as a titania precursor. To the author's knowledge, this is one of the first studies to utilize TiO_2 recovered from flocculated sludge for the preparation of LISs. Later, we compared their adsorption performance with HTO developed from commercially available NP400. The physicochemical attributes of the synthesized LTO and HTO were characterized via powder X-ray

diffraction (XRD) and scanning electron microscopy (SEM). Finally, we have used a synthetic LiOH model solution to estimate the Li sorption capacity, selectivity, and stability of the synthesized HTOs.

2 Materials and Methods

2.1 Materials

The precursors of Li_2TiO_3, lithium carbonate powder (Li_2CO_3, Assay: 99.99% trace metals basis), and NP400 (Anatase TiO_2), were purchased from Sigma-Aldrich (AU) and Bentech Frontier Co. Ltd. (Gwangju, South Korea), respectively. Hydrochloric acid (HCl, Assay: 37%) procured from Sigma-Aldrich (AU) were used for the acid pickling and regeneration of LISs. Finally, lithium hydroxide powder (LiOH, Assay: ≥ 98%) from Sigma-Aldrich (AU) was utilized to evaluate the adsorption performances of the synthesized nanoparticles. All the compounds listed were reagent-grade, and they were used without further purification. Throughout the experiment, Milli-Q water was used.

2.2 Preparation of anatase TiO_2 from dried sludge

Dry sludge produced from synthetic wastewater resembling secondary sewage effluent (SSE) and dye wastewater (DWW) obtained from a wastewater treatment plant in Daegu, South Korea, was used to make anatase TiO_2. The prepared SSE's detailed composition can be found elsewhere [59]. The chemical contents and molecular weight distributions of the synthetic wastewater produced are shown in Table 1. The components of the SSE were chosen in such a manner that the predominant organic matter had a broad molecular weight distribution. In brief, large molecular mass organic substances were provided by tannic acid, sodium lignin sulfonate, sodium lauryle sulfate peptone, and arabic acid, whereas small molecular mass organic substances were contributed by peptone, beef extract, and humic acid [49, 59].

Table 1. Constituents of the prepared synthetic SSE[as]

Compounds	Concentration (mg/L)	Fraction by organic matter	Molecular wt. (Da)
Beef extract	1.8	0.065	300,100,70

Peptone	2.7	0.138	34300,100,80
Humic acid	4.2	0.082	1,500,300
Tannic acid	4.2	0.237	6300
Sodium lignin sulfonate	2.4	0.067	12100
Sodium lauryle sulfate	0.94	0.042	34300
Arabic gum powder	4.7	0.213	900,300
Arabic acid (polysaccharide)	5	0.156	38900
$(NH_4)_2SO_4$	7.1	-	-
K_2HPO_4	7	-	-
NH_4HCO_3	19.8	-	-
$MgSO_4.7H_2O$	0.71	-	-

[a]SSE: Secondary sewage effluent

When it came to the DWW, the following physicochemical characteristics were observed: pH = 11.70; COD = 449 mg/L; TN = 72 mg/L; and TP = 3.2 mg/L in the plant's ambient environment [52]. To coagulate and flocculate SSE and DWW, 20 wt.% $TiCl_4$ was produced, and the optimum dosage from our prior study was used [49, 52, 59]. A conventional jar test was carried out, with the spinning at 100 rpm for 1 min and then at 30 rpm for 20 min. The flocculated wastewater was then dried for 48 h at 100 °C in a laboratory oven before being crushed into powder using a mortar and pestle. Later, to obtain anatase titania, the powdered materials were burned for 2 h at 600 °C. The synthesized anatase TiO_2 from SSE and DWW are termed as S-TiO_2 and D-TiO_2, respectively.

2.3 Synthesis of Li_2TiO_3 and H_2TiO_3

Anatase-type TiO_2 (S-TiO_2, and D-TiO_2) and Li_2CO_3 (2:1 Li/Ti molar ratio) were combined, crushed in an agate mortar for 20 min, and calcined in air at constant 750 °C for 4 h (ramp 12 °C/min), as reported in several previous works [17, 24, 60]. Moreover, LTO was prepared by using commercially available NP400 to compare the performance results. Later, the samples were stored in an alumina crucible kept in a desiccator to cool down to room temperature. After bringing the LTO powder to room temperature, it was crushed using a mortar and pestle. To produce HTOs, the synthesized LTOs (S-LTO, D-LTO, and NP-LTO) shown in Table 2 were dispersed in 0.2 M HCl solution (1 g/L) at room temperature for 24 h to exchange Li^+ with H^+. The dispersion was vacuum-filtered and rinsed with Milli-Q water to produce a neutral pH, and then oven-dried at 80 °C for an additional 12 h to get the final HTOs (S-HTO, D-HTO, and NP-HTO) as adsorbent. A 0.22 μm syringe-driven filter was used to filter the suspensions and estimate the Li^+ and Ti^{4+} contents of the filtrates using ICP-MS. Moreover, the Li^+ extraction rate in LTOs was determined by stirring 0.2 g of LTO in 200 mL HCl solution (0.2 M) at room temperature and collecting aliquots (2 mL) at various time intervals to evaluate Li^+ content.

Table 2. Nomenclature and the critical parameters of the LTOs and HTOs synthesis.

Preparation of LTOs				
Precursors	Name	Ti precursor g	Li Precursor g	Prepared Sample g
S-TiO_2 + Li_2CO_3	S-LTO	5.02	4.64	6.75
D-TiO_2 + Li_2CO_3	D-LTO	5.01	4.63	6.75
NP400 + Li_2CO_3	NP-LTO	5.00	4.62	6.65

Preparation of HTOs					
Precursors	Name	Initial sample g	Conc. HCl M	Pickling duration h	Prepared Sample g

S-LTO	S-HTO	2.00	0.20	24	1.40
D-LTO	D-HTO	2.05	0.20	24	1.48
NP-LTO	NP-HTO	2.02	0.20	24	1.41

2.4 Characterization

Powder XRD was performed on the materials using an X-ray diffractometer (Siemens D5000 diffractometer) operated at 40 kV and 24 mA with Cu Kα radiation at a scanning rate of 1° (2θ) min^{-1}. The JADE 3.0 software was used to compute the lattice constant parameters for the materials. We used the Scherrer equation (Equation 1) and Bragg's law (Equation 2) to estimate the synthesized samples' crystal size (C_D) and interplanar spacing (d).

$$C_D = \frac{K\lambda}{FWHM \times \cos\theta} \quad (1)$$

$$d = \frac{n\lambda}{2\sin\theta} \quad (2)$$

Here,

C_D	Crystallite size	nm
K	Scherrer constant, 0.9	
λ	Wavelength of the X-ray source, 0.15406	nm
FWHM	Full width half maxima	radians
θ	Peak position	radians
d	Interplanar spacing	nm
n	Order of diffraction, 1	

FullProof Suite (Version: July 2017) is utilized to perform Rietveld refinement on the raw XRD data of the synthesized LTOs. For Rietveld refinement, the atomic coordinates were adapted from Kataoka, Takahashi, Kijima, Nagai, Akimoto, Idemoto and Ohshima [61]. The Miller indices (*h, k, l*) for monoclinic (space group C2/c) Li_2TiO_3 were obtained using the PDF card no 33-0831, and the

interplanar spacing d was calculated using OriginPro 2018 from the peak analysis of the XRD data. The formulae utilized to determine the cell parameters are illustrated in Equation S1 and S2. A SEM (Zeiss Supra 55VP Field Emission) operating at 15 kV was utilized to investigate the synthesized nanoparticles' morphology. Inductively coupled plasma mass spectrometry (ICP-MS) (Agilent 4100) was used to determine the concentrations of Ti^{4+} and Li^{+} in the solutions after suitable dilutions. The Brunauer-EmmettTeller (BET) theory was used to calculate the effective surface area of the as-prepared samples. Autosorb iQ/ASiQwin, USA, was used to create the adsorption-desorption isotherms. The pore size distributions were then investigated using the desorption data in conjunction with the Density Functional Theory (DFT) framework.

2.5 Adsorption study

Adsorption studies were performed in batch beakers that included pre-determined quantities of HTOs and model solutions, and the mixtures were mixed and maintained at a consistent speed of 120 rpm for 24 h. ICP-MS was used to determine the initial and final ion concentrations (Agilent 4100). The tests were repeated three times, and the standard average was calculated, and the adsorption capacity was determined using Equation 3.

To determine the Li^{+} adsorption rate at an initial pH of about 11.7, manufactured HTOs (200 mg) were treated with 250 mL of a LiOH model solution containing 20 mg/L of Li^{+}. The suspension was agitated at room temperature, and aliquots (2 mL) were taken at various intervals of time during the experiment. The clear solutions were diluted for Li^{+} content analysis after syringe filtering (0.22 µm). The adsorption rates were compared to pseudo-first-order (Equation 4) and second-order (Equation 5) models to comment on the kinetic behavior of the fabricated materials. Additionally, 30 mg of HTO was dispersed in 40 mL of Li^{+} model solutions with varying starting Li^{+} concentrations (10 – 115 mg/L), and the suspensions were regularly agitated for 24 h to develop the adsorption isotherm. Following vacuum filtration of the suspensions, the clear solutions were tested for the presence of Li^{+} ions. Moreover, the isotherms were evaluated by using Langmuir (Equation 6) and Freundlich (Equation 7) models. A number of studies concerning Li recovery from brine with the assistance of HTO showed a selectivity pattern of $Li^{+} > Na^{+} > K^{+} > Mg^{2+} > Ca^{2+}$. For instance, Chitrakar, Makita, Ooi and Sonoda

[31] showed that Mg^{2+} showed poor selectivity despite having a smaller hydrated radius due to high dehydration energy during HTO-assisted Li recovery from NaOH added brine. Additionally, Lawagon, Nisola, Cuevas, Kim, Lee and Chung [62] reported that during HTO-assisted Li recovery in an equimolar mixture of Na^+ and Mg^{2+}, HTO showed more selectivity towards Na^+ due to the higher dehydration energy (-1921 kJmole-1) requirement of Mg^{2+}. Limjuco, Nisola, Lawagon, Lee, Seo, Kim and Chung [63] also reported similar selectivity patterns ($Li^+ > Na^+ > Mg^{2+} > K^+ \sim Ca^{2+}$) during Li^+ recovery using HTOs. Hence, to examine the impact of competing ions such as Na^+ on the Li^+ uptake performance of HTOs, a series of adsorption experiments were carried out in a model solution comprising LiOH and various concentrations of NaCl. ICP-MS was used to determine cation concentrations, as described in the analytical techniques section. The selectivity of HTO towards Li^+ was assessed using the distribution coefficient (Equation 8), separation factor (Equation 9), and concentration factor (Equation 10) to estimate its Li^+ adsorption capability.

$$Q_e = \frac{(C_0 - C_t)V_T}{M} \quad (3)$$

$$\ln(Q_e - Q_t) = -K_1 t + \ln Q_e \quad (4)$$

$$\frac{t}{Q_t} = \frac{t}{Q_e} + \frac{1}{K_2 Q_e^2} \quad (5)$$

$$\frac{C_e}{Q_e} = \frac{C_e}{Q_m} + \frac{1}{K_L Q_m} \quad (6)$$

$$\log Q_e = \frac{1}{n}\log C_e + \log K_F \quad (7)$$

$$K_D = \frac{Q_e}{C_e} \quad (8)$$

$$\alpha_{Me}^{Li} = \frac{K_D^{Li}}{K_D^{Me}} \quad (9)$$

$$CF = \frac{Q_e}{C_0} \quad (10)$$

Here,

Q_e	Equilibrium adsorption capacity	mg/g

C_0	Initial concentration of the target metal	mg/L
C_t	Concentration of the target element at time, t	mg/L
V_T	Total volume of the solution	L
M	Mass of the utilized adsorbent	g
Q_t	Adsorption capacity at time, t	mg/g
t	Duration of adsorption, t	h
K_1	Adsorption rate constant, pseudo-first-order model	h^{-1}
K_2	Adsorption rate constant, pseudo-second-order model	$gmg^{-1}h^{-1}$
C_e	Metal concentration at equilibrium	mg/L
Q_m	Theoretical maximum adsorption capacity	mg/g
K_L	Langmuir constant	L/mg
K_F	Freundlich constant	L/g
n	Freundlich coefficient	
K_D	Distribution coefficient	L/g
α^{Li}_{Me}	Separation factor	
CF	Concentration factor	L/g

2.6 Regeneration

For HTO regeneration, 1 L of 0.2 M HCl solution was dispersed with 1.0 g of Li^+ adsorbed HTOs and left at room temperature for 24 h. Later, about 30 mg of the acid-treated sample was treated with 40 mL of LiOH (115 mg/L Li^+) solution for 24 h to evaluate the reusability of the regenerated sample. The process was repeated 4 times to assess the stability of the synthesized HTOs.

3 Result and Discussion

3.1 Characterizations of LTOs and HTOs

The synthesized samples mentioned in Table 2 went through XRD analysis to evaluate the phase configurations, and the XRD patterns are illustrated in Fig. 1. Fig. 1 (a) and (b) depicted that the synthesized anatase TiO_2 (S-TiO_2 and D-TiO_2) from SSE and DWW showed dominant anatase crystal

planes of (101), (004), (200), (105), (211), and (204) (JCPDS No. 21-1272), which corresponds well with commercially available NP400 (Fig. 1 (c)) [64-66]. Later, after the solid-state reactions to form LTOs, the crystal planes of anatase TiO_2 were completely vanished, concluding the deterioration of the tetragonal anatase TiO_2 by developing a new crystal structure [17, 25]. Additionally, the Scherrer's equation was utilized to determine the crystal size of the assessed samples and is illustrated in Fig. 1 (d) . Compared to NP400 (20.97 nm), both S-TiO_2 (17.87 nm) and D-TiO_2 (15.35 nm) showed a smaller crystal size. Hence, the corresponding prepared S-LTO (32.32 nm) and D-LTO (31.89 nm) showed a smaller crystal size compared to NP-LTO (39.61 nm) (Fig. 1 (d)).

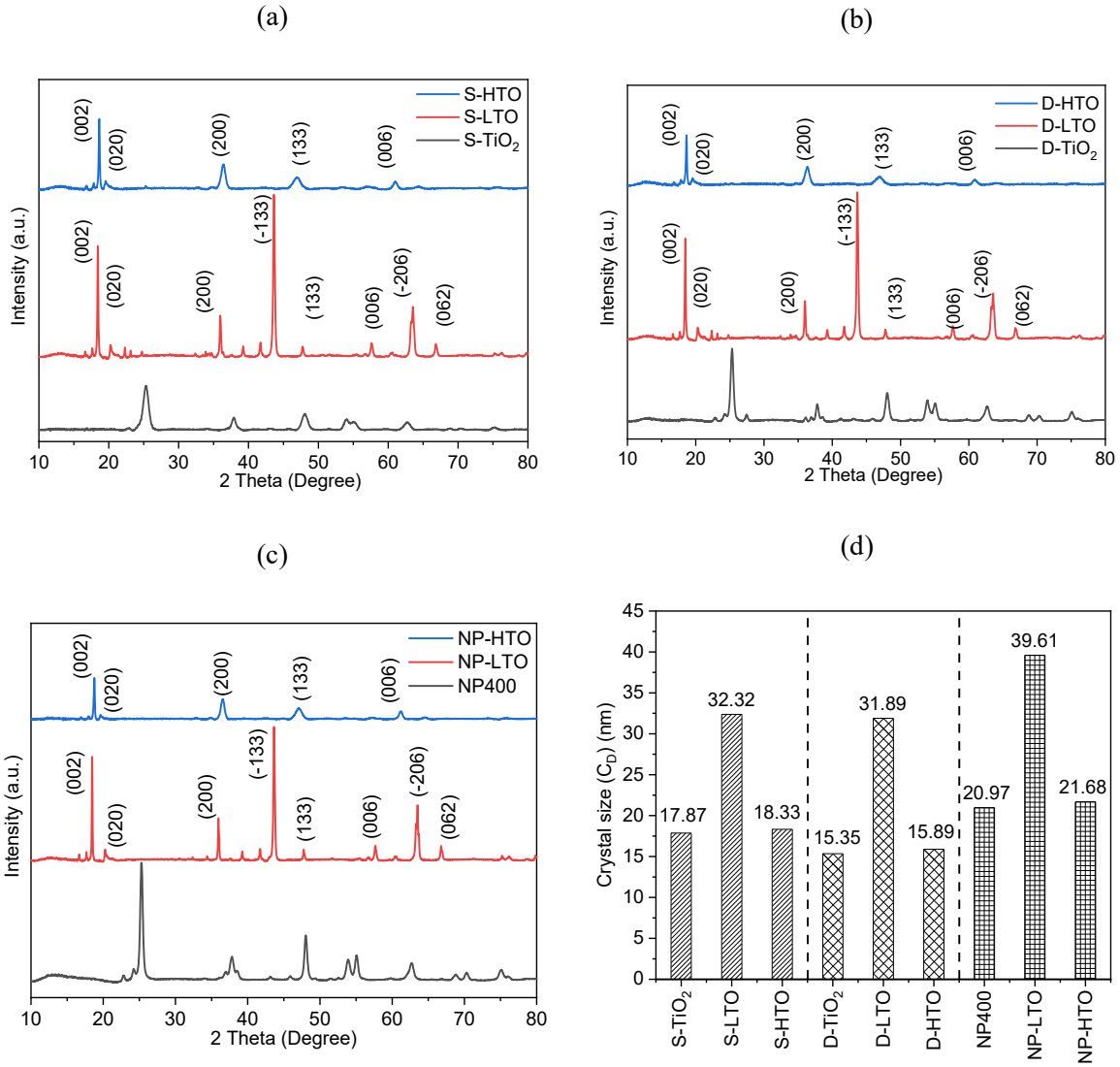

Fig. 1. XRD patterns of (a) S-TiO_2, S-LTO, and S-HTO, (b) D-TiO_2, D-LTO, and D-HTO, (c) NP400, NP-LTO, and NP-HTO, and (d) crystal sizes of the corresponding samples according to Scherrer equation.

The crystallographic data of the synthesized LTOs (S-LTO, H-LTO, and NP-LTO) are tabulated in Table 3 and compared with the standard Li_2TiO_3 structure (PDF 033-0831) [43, 67, 68]. The spectra of the prepared LTOs can be easily indexed to the pure monoclinic Li_2TiO_3 crystal (Lattice parameters: a = 0.5062 nm, b = 0.8787 nm, c = 0.9753 nm, PDF 033-0831), which is in strong harmony with published values [25]. Fig. 1 shows that all the synthesized LTOs distinctly showed the crystal planes ((002), (020), (200), (-133), (133), (006), (-206), and (062)) of monoclinic Li_2TiO_3 [38, 39, 60]. Additionally, successful HTO generation was observed from the depicted XRD patterns of S-HTO (Fig. 1 (a)), D-HTO (Fig. 1 (b)), and NP-HTO (Fig. 1 (c)) after pickling with 0.2 M HCl [28]. A flawless structure of monoclinic Li_2TiO_3 is achieved by ordering two Ti^{4+} and one Li^+ in the 4e wick-off sites in the (-133) lattice plane of the slab [69]. When the precursors are anatase TiO_2, it is possible to introduce Li^+ into the anatase cell during the solid-state reaction. Several studies, like that of Tielens, Calatayud, Beltrán, Minot and Andrés [70], have shown that the vacant deformed octahedron centred at 4b special locations is the most favored site for the occupancy of lithium during insertion. As soon as the insertion is completed, the fundamental structure of the (-133) lattice plane is established (Fig. 1). A more generic description of the crystal structure of Li_2TiO_3 is $Li[Li_{1/3}Ti_{2/3}]O_2$, in which oxygen atoms form a cubic tight packing, while metal atoms are placed in the octahedron's voids [67]. There are two layers in the layered structure of Li_2TiO_3: one Li layer, which is entirely composed of Li atoms, and another $LiTi_2$ layer, which is composed of one-third Li^+ and two-thirds Ti^{4+} atoms [60]. It has been previously shown that the H^+ generated by the hydrolysis of HCl is completely swapped with Li^+ in the Li layer, succeeded by the $LiTi_2$ layer, resulting in the formation of $H[H_{1/3}Ti_{2/3}]O_2$ [43]. Later, Li^+ in suspension will no longer be able to re-shuffle with H^+ in the ($H_{1/3}Ti_{2/3}$) layer; but, if the H layer is present, it will be able to re-exchange with H^+ in the H layer. As a result, LTO's lithium adsorption capacity is considerably lower than its theoretically predicted value [2, 37, 43].

Fig 1 (a – c) depicted that the HTO samples displayed a similar trend to the LTOs in diffraction peaks, but the signals were slightly weaker. Furthermore, the HTO peaks (2θ) moved marginally to the right (~18.40° to ~18.60° and ~35.90° to ~36.50°). As a result, the diffraction peaks of crystal planes (020) and (002) are altered, while the diffraction peaks of crystal planes (133) and (006) are broadened. This shows that Li^+ and H^+ binding modes in the Ti-O layer are distinct. The particle size decreases after pickling due to ion exchange between H^+ (radius 0.0012 nm) with a lower ionic radius and Li^+ (radius 0.076 nm) with a larger ionic radius [28]. After acid pickling, the lattice plane created by the insertion of Li^+ into the TiO_2 lattice vanishes, as does the diffraction peaks (-206) and (062), showing that Li^+ has been extracted from LTOs. The Ti-O lattice in the LTO structure is highly stable, and the Ti in the crystal structure shows its present location, despite the fact that most of the Li^+ are eliminated following acid elution, resulting in reduced grain size. This unique property is due to the stiff structure of the compound and the fact that it does not expand or contract much in an aqueous solution.

Table 3. Crystallographic data for synthesized samples.

Sample name	PDF 033-0831	S-LTO	D-LTO	NP-LTO
Structural Formula	Li_2TiO_3	Li_2TiO_3	Li_2TiO_3	Li_2TiO_3
Crystal system	Monoclinic	Monoclinic	Monoclinic	Monoclinic
		Lattice parameters		
a (Å)	5.062	5.063	5.061	5.069
b (Å)	8.787	8.830	8.823	8.813
c (Å)	9.753	9.814	9.808	9.884
β (°)	100.212	100.202	100.238	100.730
Cell volume $(Å)^3$	427.010	431.845	431.023	433.815
(a)		(b)		(c)

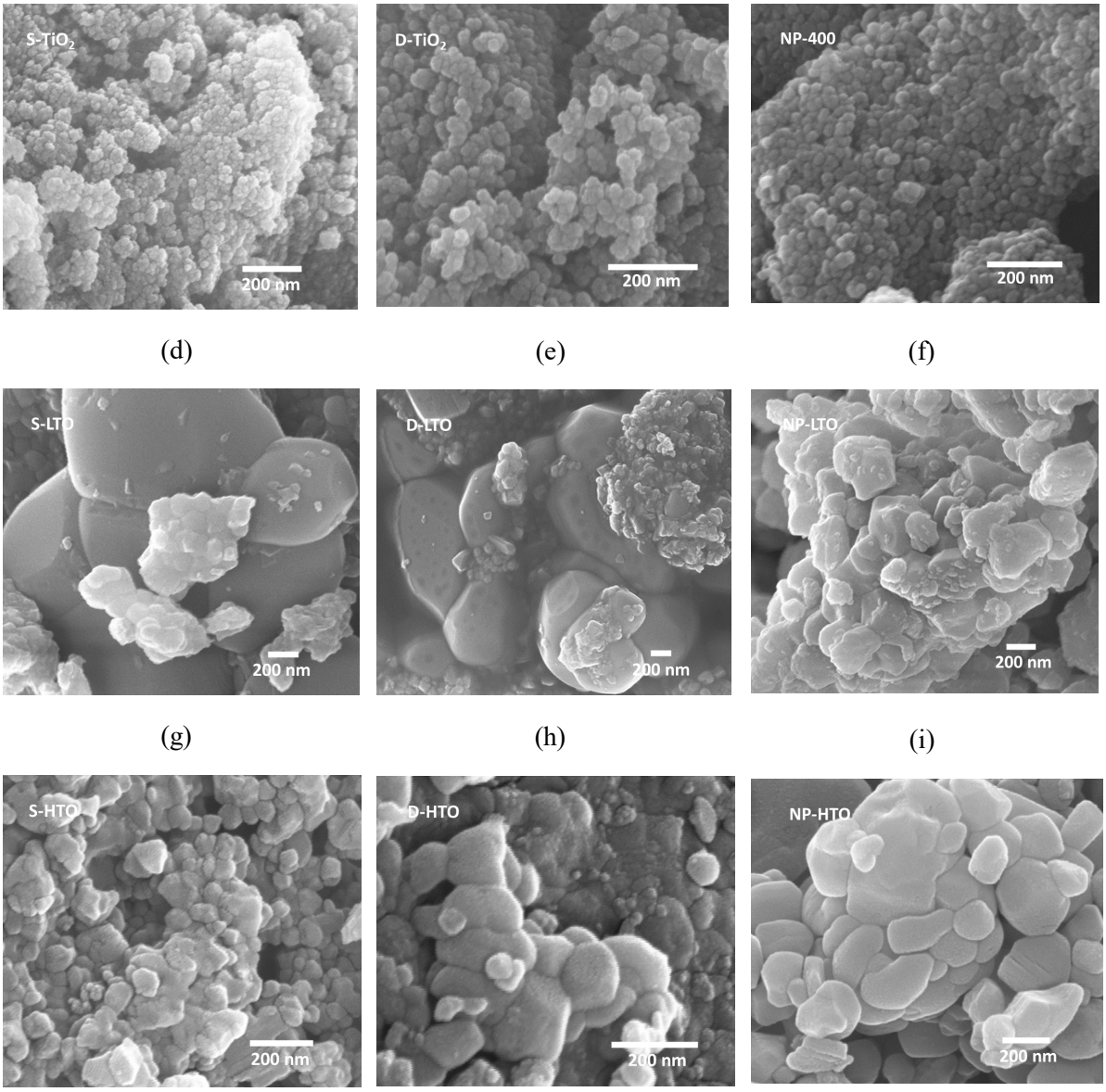

301 Fig. 2. SEM image of utilized anatase TiO_2 (a – c), synthesized LTOs (d – f), and HTOs (g – i).

302 The SEM images of the utilized anatase TiO_2 along with the synthesized LTOs and HTOs are
303 depicted in Fig. 2. Along with NP400, the synthesized anatase S-TiO_2 and D-TiO_2 showed spherical
304 morphology (Fig. 2 (a – b)). However, partial aggregations of numerous particles with irregular shapes
305 have been seen in S-TiO_2 and D-TiO_2, which is thought to be due to the materials' ability to retain their
306 distinctive sludge morphology even after calcination [52, 53]. In the S-TiO_2 sample, nanoparticles with
307 a spherical form were found in the 17 – 23 nm size range, which corresponds well with the XRD results.
308 The D-TiO_2 sample, on the other hand, included spherical nanoparticles with sizes ranging from 15 to
309 30 nm, which were determined to be amorphous. These findings reveal that the wastewater quality has
310 an influence on the shape, size, and morphology of TiO_2 produced in a microcosm context. Previous
311 research has shown that particle agglomeration may make ion exchange sites in the solution challenging
312 to reach [2]. However, according to the XRD analysis, the 2nd calcination for LTO generation and 24 h

of stirring in 0.2 M HCl at room temperature effectively produced HTOs (see Fig. 2 (d – i)). As shown in Fig. 2 (d – f), the S-LTO and D-LTO samples generated by the solid-state reaction are relatively homogenous and have a particle size of around 0.5 µm – 1.5 µm. However, there was a lot of aggregation in NP-LTO. According to our findings, it is possible that the hydrothermal preparation procedure for commercial NP400 reduced the crystallinity of the sample, resulting in poor LTO and a consequent reduction in adsorption capacity. As illustrated in Fig. 2 (g – i), particle size changes somewhat after acid pickling to form HTOs. While Li^+ is eluted by acid, this might be caused by the exchange of H^+ and Li^+ in the unit cell, which would cause the unit cell to shrink [2, 24] . Past works showed although the interplanar spacing of the acid pickled sample was decreased, the crystal morphology was intact; nonetheless, some of the smooth surfaces became coarse, showing that despite the extraction of Li^+ ions from the intralayer, the pickling procedure did not materially impair the particle [25].

Nitrogen adsorption-desorption curves performed at 77 K were developed to assess the variation in effective surface areas of the synthesized HTOs from different precursors. The N_2 adsorption-desorption isotherms, along with BET surface area (S_{BET}) and DFT pore size distribution data, are presented in Fig. 3 (a – c). The multipoint BET analysis found S_{BET} values of 24.45 m^2/g, 37.61 m^2/g, and 39.78 m^2/g for NP-HTO, S-HTO, and D-HTO, respectively (Fig. 3 (b)). The smaller crystal size of S-HTO and D-HTO illustrated in Fig. 1 (d) corresponds with the S_{BET} values. Irrespective of the precursor TiO_2, all the synthesized HTOs, showed type-IV and H3 hysteresis loop, which confirms the appearance of mesopores [71]. Moreover, the performed DFT analysis showed the mode pore diameters for the synthesized HTOs are above 2 nm, confirming the presence of mesopores (Fig. 2 (c)) [72]. The increased effective surface areas of S-HTO and D-HTO could be attributed to the doped C atoms of the precursor TiO_2, which caused the initial reduced crystal size [49, 64, 66].

(a)

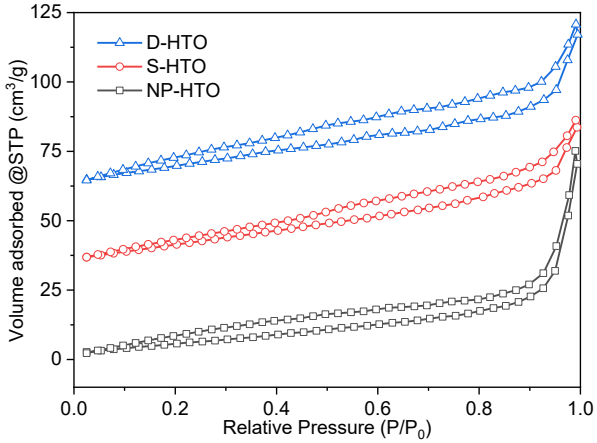

(b)

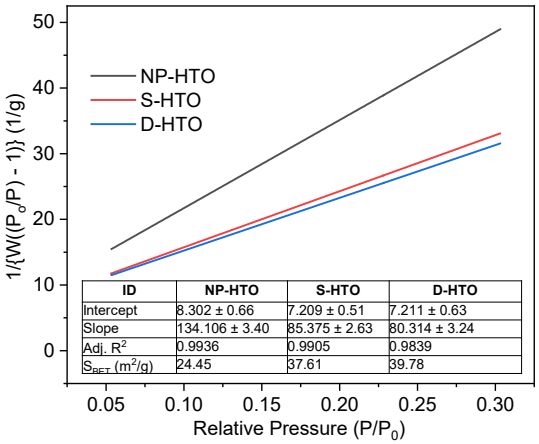

ID	NP-HTO	S-HTO	D-HTO
Intercept	8.302 ± 0.66	7.209 ± 0.51	7.211 ± 0.63
Slope	134.106 ± 3.40	85.375 ± 2.63	80.314 ± 3.24
Adj. R^2	0.9936	0.9905	0.9839
S_{BET} (m^2/g)	24.45	37.61	39.78

(c)

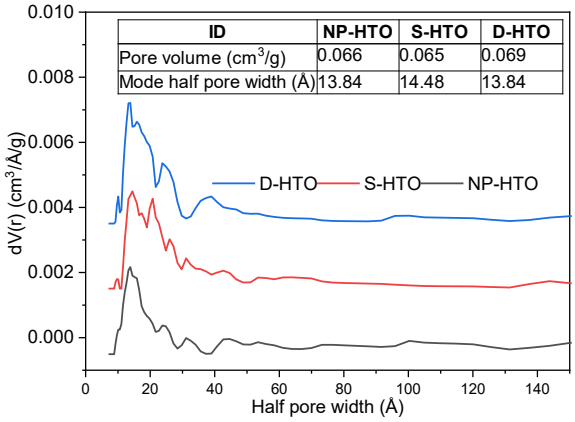

Fig. 3. (a) N_2 adsorption-desorption isotherms, (b) multipoint BET analysis, and (c) DFT pore size distributions for synthesized D-HTO, S-HTO, and NP-HTO.

3.2 Adsorption

3.2.1 Adsorption kinetics

The kinetics of Li^+ adsorption in synthesized HTOs were studied in order to estimate the Li^+ extraction rate, which determines the required process duration. The kinetic data is significant because it is used to build batch reactors, fixed-bed reactors, and other flow-through operations [28]. Furthermore, adsorption kinetics is crucial to better understand the adsorption process and is often used to investigate the adsorption mechanism [24, 62, 73]. As a result, the Li^+ adsorption characteristics of the produced HTOs (S-HTO, D-HTO, and NP-HTO) were studied in a model LiOH (20 mg/L) solution at the initial pH of ~11.70. The relationship between Li^+ adsorption capability and adsorption time in HTOs is investigated and illustrated in Fig. 4. As shown in Fig. 4 (a) and (b), the Q_e of HTOs in LiOH solution increased over time in proportion to the decrease in pH caused by deprotonation. During the first 8 h, the Q_e of HTOs rose quickly and gradually approached equilibrium. The equilibrium adsorption capacities of S-HTO, D-HTO, and NP-HTO were calculated as 16.87, 15.45, and 14.60 mg/g, respectively, while the respective equilibrium pH was 8.01, 7.70, and 9.20. When compared to sludge-generated HTOs, the high equilibrium pH of NP-HTO indicated its poor adsorption capability. In order to determine the overall rate of adsorption in HTOs, pseudo-first-order (Equation 4) and pseudo-second-order (Equation 5) models were employed [6, 17, 25], and the results are depicted in Fig. 3 (c) and Table 3. From Fig. 4 (c), it can be seen that the pseudo-second-order model has more successfully characterized the adsorption findings for all of the HTOs. The results showed that the R^2 coefficient for

all synthesized HTOs is greater than the R^2 coefficient for the pseudo-first-order kinetic model, reaching $R^2 > 0.99$. So, it can be concluded that the adsorption of S-HTO, D-HTO, and NP-HTO in solution is more consistent with the pseudo-second-order kinetic model than with other models. The computed K_2 of S-HTO, D-HTO, and NP-HTO were estimated to be 0.083, 0.110, and 0.009 $g.mg^{-1}h^{-1}$, respectively, using the pseudo-second-order kinetic equation. Furthermore, the calculated constants (Table 4) show that the theoretical Q_e obtained from pseudo-second-order kinetics is similar to the actual value. Meanwhile, as seen in Fig. 4 (c), the pseudo-first-order model was only viable during the early phase of the reaction; as the adsorption process reached equilibrium, the model significantly differed from the experimental findings. Because the experimental findings match the model's predictions, this model may be used to explain the total rate of adsorption on Li^+ in prepared HTOs. As a result, chemisorption dominates the adsorption processes associated with the produced HTOs. Studies have shown that Li^+ adsorption on HTOs occurs in three steps, viz., (a) Li^+ propagation from the aqueous medium, (b) Li^+ diffusion via HTOs, and (c) direct Li^+ adsorption on HTO's active sites [74].

(a)

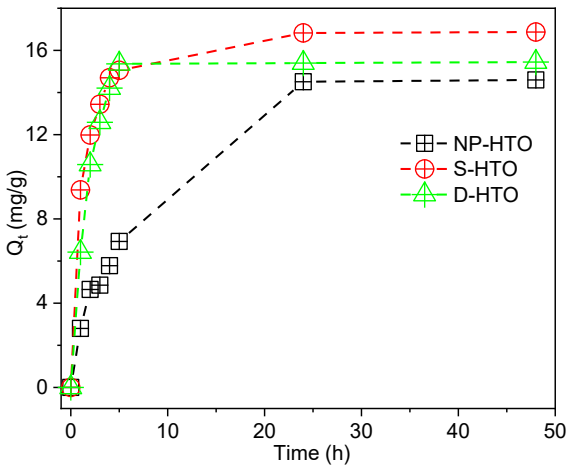

(b)

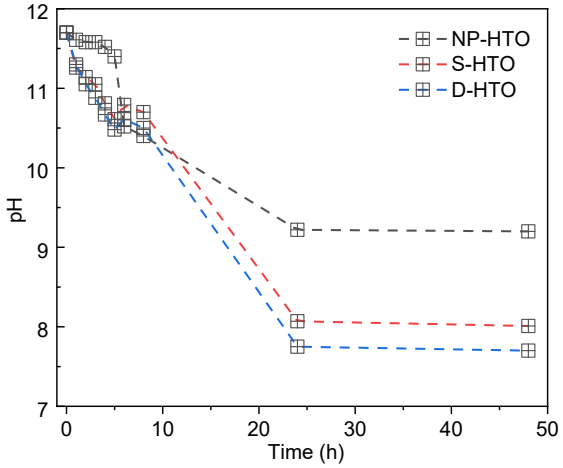

(c)

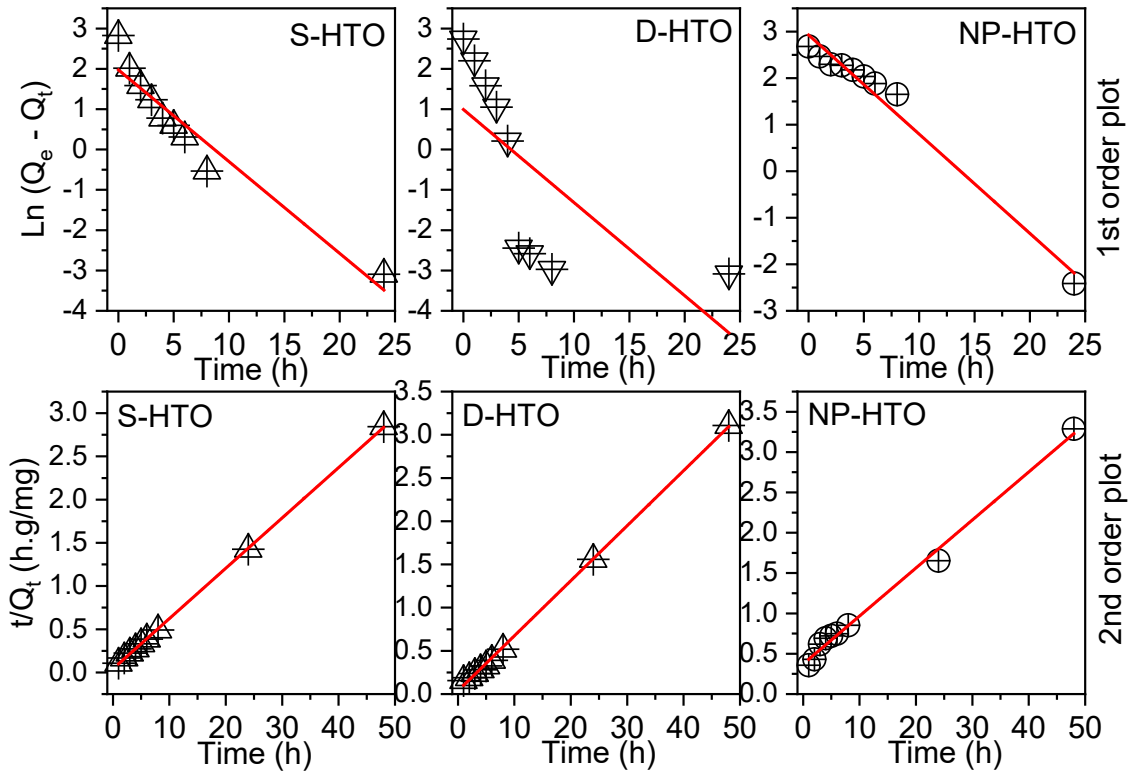

370 Fig. 4. Adsorption kinetics of S-HTO, D-HTO, and NP-HTO showing Q_e vs h and pH vs h plots; (c)
371 Pseudo-first-order and second-order plots of S-HTO, D-HTO, and NP-HTO (Initial pH = 11.7, C_0 = 20
372 mg/L, V_T = 250 mL, and M = 200 mg).

373 Table 4. Kinetic parameters of the synthesized S-HTO, D-HTO, and NP-HTO, illustrating the
374 experimental and theoretical Q_e.

Adsorbent	Pseudo-first-order			Pseudo-second-orders			
	Experimental Q_e mg/g	K_1 h^{-1}	R^2	Theoretical Q_e mg/g	Experimental Q_e mg/g	K_2 $g.mg^{-1}.h^{-1}$	R^2	Theoretical Q_e mg/g

S-HTO	16.87	0.00948	0.91847	7.21	16.87	0.0831	0.9999	17.17
D-HTO	15.45	0.00962	0.41471	2.7	15.45	0.1101	0.999	15.7
NP-HTO	14.6	0.00888	0.97107	18.7	14.6	0.0095	0.9918	16.8

375

376 3.2.2 Li^+ adsorption isotherm

377 The adsorption isotherm models developed by Langmuir and Freundlich are the most frequently
378 used models for investigating adsorption isotherms. To summarize, the Langmuir model implies that
379 adsorbents absorb cations in monolayers and the adsorption energy is constant at each exchange site
380 [67]. On the other hand, the Freundlich model is deemed to represent multilayer adsorption, which is
381 an empirical equation developed from experimental data [42, 75]. The corresponding equations are
382 shown in Equation 6 and 7. LiOH model solutions with varying concentrations were analyzed, and the
383 initial Li^+ concentration and the equilibrium adsorption capacity of the adsorbent were calculated using
384 the Langmuir and Freundlich isothermal adsorption equation. Fig. 5 (c) and Table 5 show the findings
385 as well as the associated adsorption isothermal parameters. The correlation coefficients of the
386 synthesized HTOs match the Langmuir equation better than the Freundlich equation, as seen in Table
387 5. This indicates that a monolayer of Li^+ was adsorbed on a set number of identical and localized sites
388 inside the HTO lattice, in contrast to the Freundlich model, which implies a heterogeneous adsorbent
389 surface. Langmuir adsorption isotherm constants (Table 5) revealed Q_m of 33.08, 34.36, and 21.66 mg/g
390 for S-HTO, D-HTO, and NP-HTO, respectively.

(a) (b)

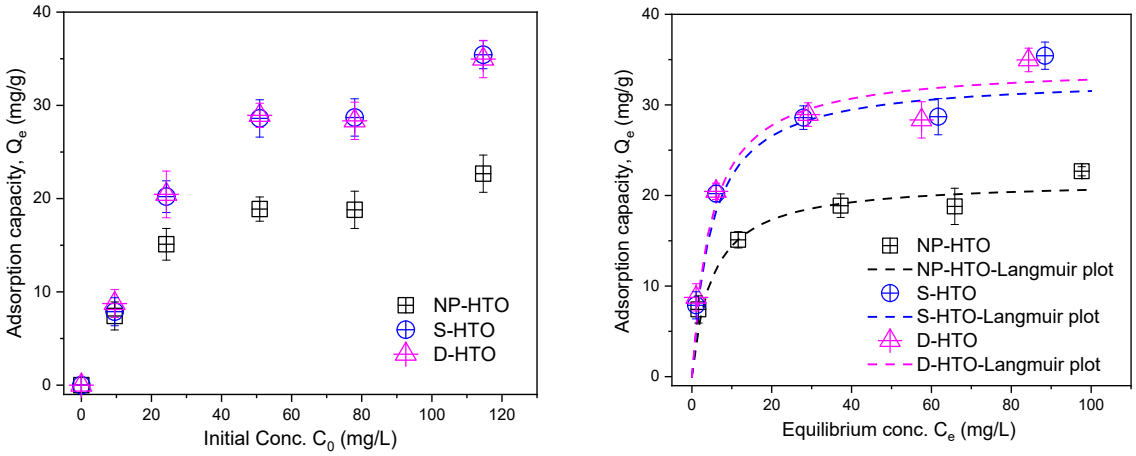

(c)

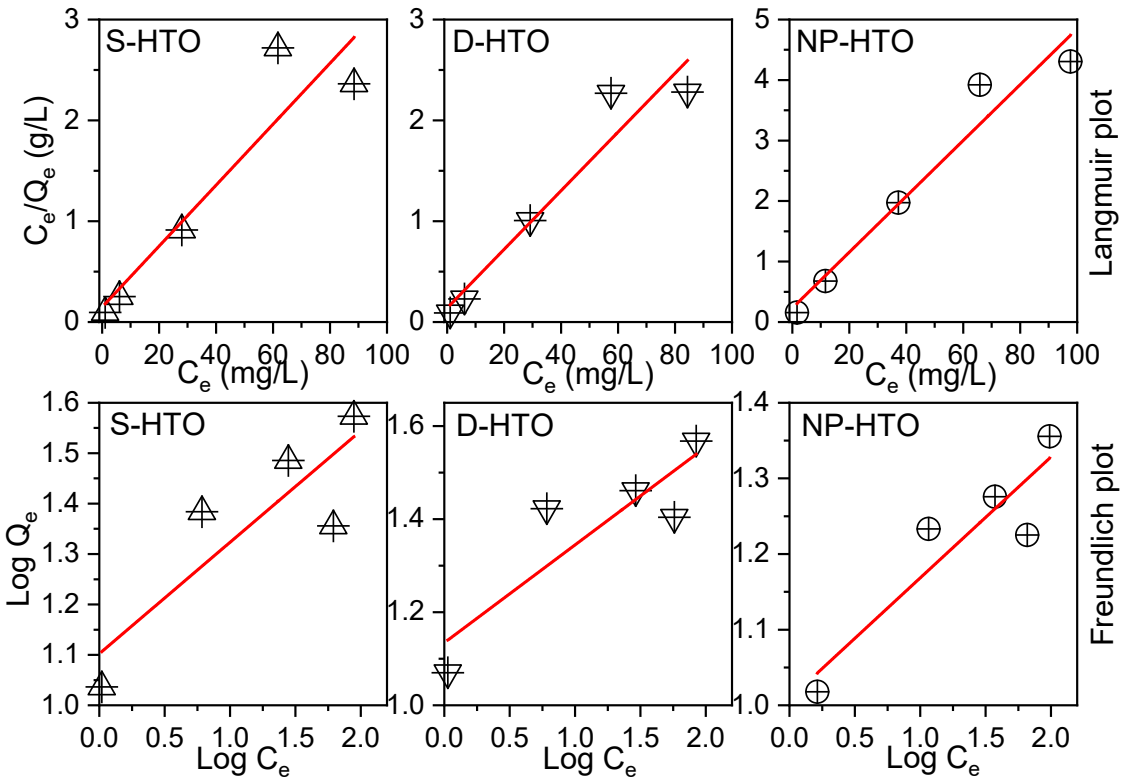

391 Fig. 5. Adsorption isotherms of the synthesized S-HTO, D-HTO, and NP-HTO, showing Q_e vs C_0 (a),
392 and Q_e vs C_e; (c) Langmuir and Freundlich isotherms of S-HTO, D-HTO, and NP-HTO in LiOH model
393 solution (C_0 = 0 – 115 mg/L, V_T = 40 mL, and M = 30 mg).

394 Table 5. Parameters of Langmuir and Freundlich isothermal adsorption model.

Adsorbent	Langmuir			Freundlich			
	Experimental Q_m mg/g	K_L L/mg	R^2	Theoretical Q_m mg/g	Experimental Q_m mg/g	K_F L/g	n	R^2
S-HTO	35.43	0.203651	0.83376	33.08	37.43	12.65465	4.522022	0.65962
D-HTO	34.97	0.209127	0.9056	34.36	36.97	13.62511	4.754207	0.70108
NP-HTO	22.67	0.19981	0.93886	21.66	22.67	10.19906	6.252345	0.78351

395

396 3.3 Stability, reusability and selectivity

397 A promising Li^+ adsorbent must have excellent performance stability in order to be used over an
398 extended period of time. The reusability of the produced HTOs (S-HTO and D-HTO) was assessed in
399 terms of Q_e after multiple adsorption-desorption cycles at a solid-to-liquid ratio less than 1. In a 115
400 mg/L LiOH model solution for 24 hours, the equilibrium adsorption capacity of the synthesized S-HTO
401 and D-HTO was determined. Following that, Li^+ desorption and HTO regeneration was carried out
402 using a pickling solution of 0.2 M HCl (1 g/L). In terms of Q_e, the findings show that repeated acid
403 treatment had minimal effect on S-HTO and D-HTO's performance (see Fig. 6. (d)). It performed
404 consistently, with an average Q_e of 34.88 and 34.50 mg/g for S-HTO and D-HTO, respectively. The
405 quantity of Ti^{4+} dissolution by the 0.2 M HCl solution was measured for an extended length of time to
406 evaluate the acid resistance of the produced HTOs. In addition, the kinetics of Li^+ extraction in LTOs
407 were investigated at various intervals, as shown in Fig. 6 (a – c). Previous research revealed that at an
408 H^+/Li^+ molar ratio of 1.0, almost 100% of the lithium was extracted; however, the pace was sluggish,
409 taking 1 d for complete Li^+ extraction. Other studies found sluggish Li^+ extractability rates in
410 monoclinic Li_2TiO_3 precursors; almost complete lithium extraction (~ 100%) was obtained from

411 Li_2TiO_3 in 0.5 M HNO_3 by changing acid every day for 14 d at ambient temperature or in 0.1 M HCl
412 for 3 d at 60 °C [31]. The extended calcination duration of the Li_2TiO_3 precursors (calcination at 700 °C,
413 24 h) compared to the current LTOs (this study) (calcination at 750 °C, 4 h) is anticipated to result in a
414 prolonged lithium extractability rate in Li_2TiO_3. As can be seen from Fig. 6 (a – c), the rate of Li^+
415 extracted reached 85.55% (108.22 mg/g Li^+), 84.39% (106.75 mg/g Li^+), and 79.12% (100.11 mg/g Li^+)
416 for S-LTO, D-LTO, and NP-LTO, respectively, whereas the respective Ti^{4+} dissolution was 0.63%,
417 0.71%, and 2.49%. Hence, for all the LTOs high rate of Li^+ extraction was observed in the initial 8 h
418 and negligible Ti^{4+} dissolution. However, even after 72 h pickling, none of the LTOs reached 100% Li^+
419 extraction. The LISs reached around 95% Li^+ extraction after 72 h of HCl pickling. Interestingly,
420 compared to NP-LTO, the sludge-generated LTOs showed more stability regarding Ti^{4+} dissolution at
421 the end of 72 h acid treatment, which was 2.38%, 2.44%, and 12.67% for S-HTO, D-HTO, and NP-
422 HTO, respectively. A significant Ti^{4+} loss indicates that HTO is deteriorating, which may have an
423 impact on its long-term adsorption capability and the number of effective adsorption sites. As a result,
424 S-HTO and D-HTO showed better adsorption capability. Other kinds of LIS, such as LMOs, are less
425 stable in acid solutions due to significant Mn^{2+} elution. As a result, the synthetic HTOs (S-HTO and D-
426 HTO) had a better chemical resistance, indicating that this adsorbent may outlive the LMOs.

(a) (b)

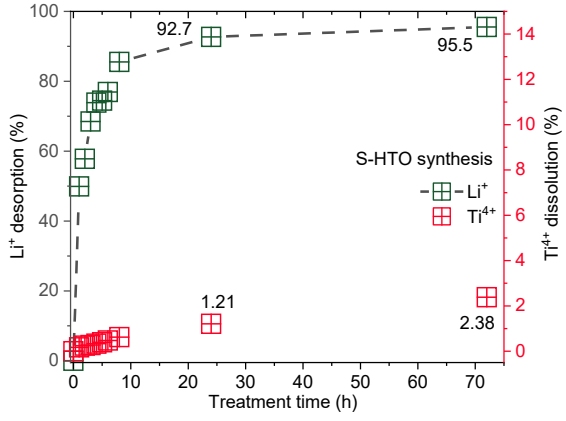

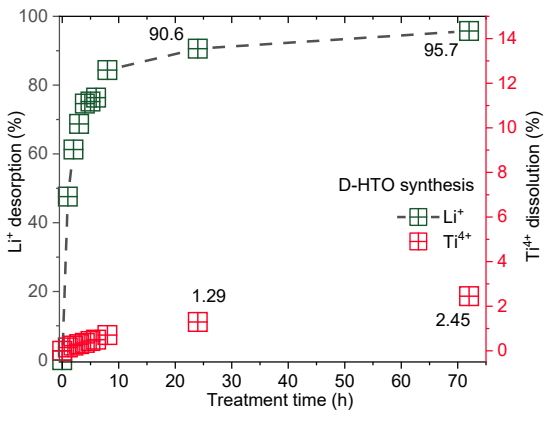

(c) (d)

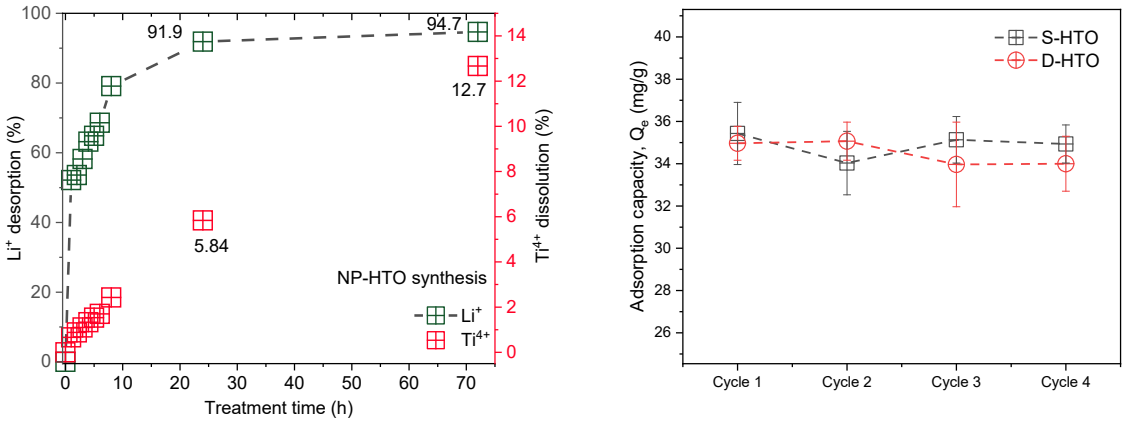

427 Fig. 6. Ti^{4+} dissolution and Li^{+} extraction curves during acid pickling for (a) S-HTO, (b) D-HTO, (c)

428 NP-HTO; (d) recyclability performance of the synthesized S-HTO and D-HTO in LiOH model solution

429 (Pickling acid = 0.2 M HCl, S/L = 1 g/L, duration = 72 h (acid pickling), 24 h (regeneration)).

Table 6. Li^+ selectivity of S-HTO, D-HTO, and NP-HTO in the presence of varying concentration of Na^+(C_0 = 115 mg/L, V_T = 40 mL, M = 30 mg).

	Li^+ adsorption					Na^+ adsorption					α^{Li}_{Na}
	C_0 mg/L	C_e mg/L	Q_e mg/g	K_D L/g	CF L/g	C_0 mg/L	C_e mg/L	Q_e mg/g	$K_D \times 10^{-3}$ L/g	CF × 10^{-3} L/g	
S-HTO	114.70	86.25	37.94	0.44	0.33	0.00	0.00	0.00	0.00	0.00	0.00
	116.30	89.34	35.94	0.40	0.31	730.99	730.74	0.87	1.19	1.19	337.45
	115.70	88.62	36.11	0.41	0.31	1373.73	1372.26	5.00	3.64	3.64	112.03
	114.10	87.56	35.38	0.40	0.31	2713.95	2711.84	7.14	2.63	2.63	153.63
D-HTO	115.20	86.43	38.35	0.44	0.33	0.00	0.00	0.00	0.00	0.00	0.00
	115.40	86.87	38.04	0.44	0.33	764.37	763.86	1.71	2.24	2.24	195.90
	114.70	87.79	35.88	0.41	0.31	1398.48	1397.08	4.75	3.40	3.40	120.33
	116.10	91.53	32.75	0.36	0.28	2654.50	2651.77	9.25	3.49	3.48	102.69
NP-HTO	115.70	97.95	23.66	0.24	0.20	0.00	0.00	0.00	0.00	0.00	0.00
	114.20	97.08	22.82	0.24	0.20	632.81	632.66	0.51	0.80	0.80	293.03
	116.60	99.69	22.54	0.23	0.19	1367.54	1367.30	0.81	0.59	0.59	381.05
	115.00	98.72	21.70	0.22	0.19	2478.76	2478.44	1.08	0.44	0.44s	504.61

After salt precipitation, the Li-containing precursors include additional metal ions, such as Na^+ and K^+, in addition to Li^+, when extracting Li^+ from brine using the adsorption technique to create lithium compounds [24, 31]. As a result, it is critical to look into the impact of competing ions on the adsorption capacity of our sludge-generated HTOs. A binary mixture of Li^+ and Na^+ salt with changing Na^+ concentration was the simulated model solution investigated in this study. Table 6 illustrated, even at a very high concentration (> 2200 mg/L) of Na^+, the adsorption capacity for Li^+ in the solution containing Li^+ and Na^+ reached 35.38, 32.75, and 21.70 mg/g for S-HTO, D-HTO, and NP-HTO, respectively. As a result, the presence of Na^+ in the model solution had minimal impact on the adsorption capacity of the synthesized HTOs. Furthermore, the exchange capacity for Na^+ was limited (see K_D values in Table 6). Additionally, Table 6 shows the Na^+ separation coefficients in the Li-containing solution, which are much higher than 1. The findings further show that the HTOs produced from sludge has a very high selectivity for Li^+. Several studies showed the hole in the structure could only accept ions with matching ionic radii due to the memory effect of LISs during ion exchange. Consequently, Na^+ (0.095 nm) ionic radius is significantly high compared to Li^+ (0.060 nm), which is not advantageous to the hole of the produced HTOs. The presence of coexisting Na^+ had no significant impact on the adsorption performance of S-HTO and D-HTO on Li^+, indicating that these compounds may be a viable option for Li^+ recovery in the near future.

The adsorption capacity of the synthesized HTOs was assessed in the presence of the competing cations (Na^+, K^+, Mg^{2+}, and Ca^{2+}) in an equimolar (10 mM) solution at Li+ concentration lower than 100 mg/L to obtain the adsorption performance in lower grade brine. Fig.7 (a) and Table S4 illustrated the adsorption performances of the synthesized HTOs from various precursors. The results (Fig. 7 (a)) revealed that after 24 h of ion exchange, the maximum Li^+ removal of the prepared HTOs followed this order: D-HTO (28.54 mg/g) > S-HTO (27.77 mg/g) > NP-HTO (19.94 mg/g), which reflects a similar trend as with the SBET values. Both of the sludge-generated TiO_2 were found extensively selective towards Li^+. By considering the separation factors, the selectivity sequence showed the following trend, $Li^+ > Mg^{2+} > Na^+ > Ca^{2+} > K^+$. Perhaps due to having a similar ionic radius, Mg^{2+} (0.065 nm) showed some affinity for ion exchange [28, 42, 60]. However, due to the substantially high dehydration energy

of 1921 kJ/mol, the penetration through the HTO lattice was limited [76]. On the other hand, for both sludge-generated HTOs, K+ showed the maximum α^{Li}_{Me} value dedicated to the large ionic radius of 0.133 nm. Moreover, the adsorption of the competing ions could be dedicated to the physisorption only rather than ion exchange, as the BET analysis showed mild microporosity of the HTO samples [31].

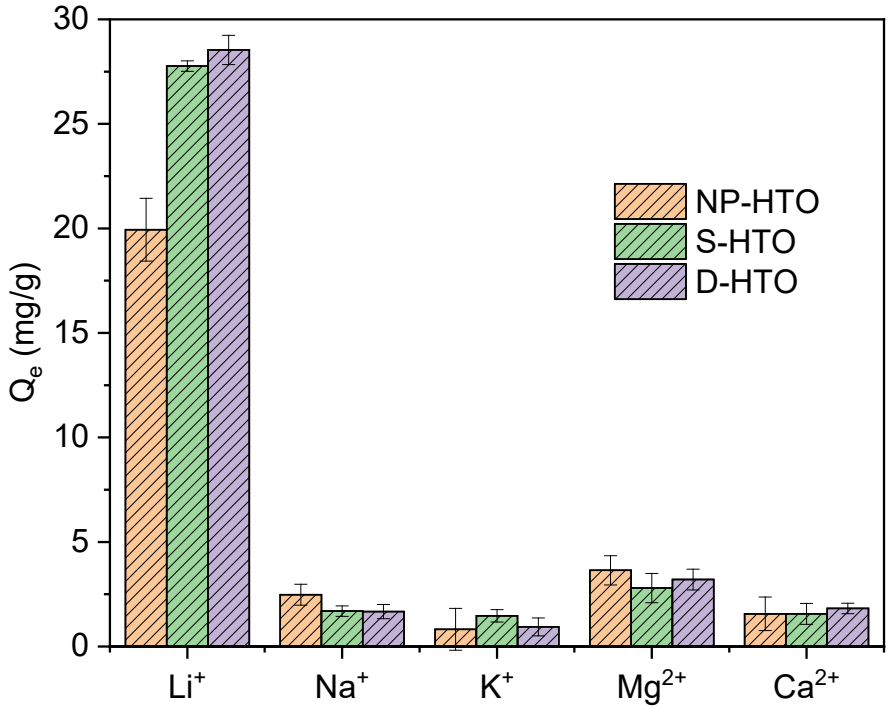

Fig. 7. Adsorption capacity of the synthesized HTOs in presence of the competing coexisting ions (C_0 = 58.42 mg/L (< 100 mg/L), V_T = 40 mL, M = 30 mg).

4 Conclusions

A monoclinic spinal Li_2TiO_3 was prepared using a solid-state reaction in between sludge-generated anatase TiO_2 and Li_2CO_3 as precursors. After 0.2 M HCl treatment of 24 h, LISs were prepared with Li^+ extraction rates of 92.70% and 90.60% for S-HTO (LIS generated from synthetic wastewater) and D-HTO (LIS generated from dye wastewater), respectively. Moreover, a 72 h acid treatment showed minimal Ti^{4+} dissolution of 2.38% and 2.45%, confirming the durability of the synthesized LISs. A number of batch adsorption experiments were carried out on the sludge-generated LISs, which showed superior adsorption capacity and kinetics. Both S-HTO and D-HTO confirmed pseudo-second-order kinetic and Langmuir isotherm models. Additionally, the regeneration experiments depicted that even

after four reuse cycles, the average adsorption capacity was reported as ~35 mg/g for all the sludge-generated HTOs. In the presence of competing Na^+ in adsorption model solutions, the prepared LISs showed substantial selectivity towards Li^+. At a very high concentration of Na^+ (> 2200 mg/L), the Li^+ separation factors of S-HTO and D-HTO were 153.63 (>> 1) and 102.69 (>> 1) , respectively. Finally, the sludge-generated TiO_2 could be a potential anatase TiO_2 precursor to prepare powerful LISs, which could eventually be a good alternative for commercial TiO_2 precursors.

5 Acknowledgements

This research was supported by the Qatar National Research Fund under its National Priorities Research Program (NPRP 12S-0227-190166) and Smart Civil Infrastructure Research Program funded by Ministry of Land, Infrastructure, and Transport of the Korean government.

6 References

[1] R. Marthi, Y.R. Smith, Application and limitations of a H2TiO3 – Diatomaceous earth composite synthesized from titania slag as a selective lithium adsorbent, Separation and Purification Technology, 254 (2021).
[2] X. Li, Y. Chao, L. Chen, W. Chen, J. Luo, C. Wang, P. Wu, H. Li, W. Zhu, Taming wettability of lithium ion sieve via different TiO2 precursors for effective Li recovery from aqueous lithium resources, Chemical Engineering Journal, 392 (2020).
[3] L. Li, V.G. Deshmane, M.P. Paranthaman, R. Bhave, B.A. Moyer, S. Harrison, Lithium Recovery from Aqueous Resources and Batteries: A Brief Review, Johnson Matthey Technology Review, 62 (2018) 161-176.
[4] A. Siekierka, M. Bryjak, Selective sorbents for recovery of lithium ions by hybrid capacitive deionization, Desalination, 520 (2021).
[5] U. Kamran, S.-J. Park, Hybrid biochar supported transition metal doped MnO2 composites: Efficient contenders for lithium adsorption and recovery from aqueous solutions, Desalination, 522 (2022).
[6] U. Kamran, S.-J. Park, Functionalized titanate nanotubes for efficient lithium adsorption and recovery from aqueous media, Journal of Solid State Chemistry, 283 (2020).
[7] D. Fasel, M.Q. Tran, Availability of lithium in the context of future D–T fusion reactors, Fusion Eng. Des., 75-79 (2005) 1163-1168.
[8] R. Chitrakar, H. Kanoh, Y. Miyai, K. Ooi, Recovery of Lithium from Seawater Using Manganese Oxide Adsorbent (H1.6Mn1.6O4) Derived from Li1.6Mn1.6O4, Industrial & Engineering Chemistry Research, 40 (2001) 2054-2058.
[9] J. Zhong, S. Lin, J. Yu, Li+ adsorption performance and mechanism using lithium/aluminum layered double hydroxides in low grade brines, Desalination, 505 (2021).
[10] X. Zhao, M. Feng, Y. Jiao, Y. Zhang, Y. Wang, Z. Sha, Lithium extraction from brine in an ionic selective desalination battery, Desalination, 481 (2020).
[11] D. Liu, Z. Li, L. He, Z. Zhao, Facet engineered Li3PO4 for lithium recovery from brines, Desalination, 514 (2021).
[12] M. Ejeian, A. Grant, H.K. Shon, A. Razmjou, Is lithium brine water?, Desalination, 518 (2021).

[13] Y. Mu, C. Zhang, W. Zhang, Y. Wang, Electrochemical lithium recovery from brine with high Mg2+/Li+ ratio using mesoporous λ-MnO2/LiMn2O4 modified 3D graphite felt electrodes, Desalination, 511 (2021).
[14] H. Ambrose, A. Kendall, Understanding the future of lithium: Part 2, temporally and spatially resolved life‐cycle assessment modeling, Journal of Industrial Ecology, 24 (2019) 90-100.
[15] C. Zhang, Y. Mu, S. Zhao, W. Zhang, Y. Wang, Lithium extraction from synthetic brine with high Mg2+/Li+ ratio using the polymer inclusion membrane, Desalination, 496 (2020).
[16] H. Ambrose, A. Kendall, Understanding the future of lithium: Part 1, resource model, Journal of Industrial Ecology, 24 (2019) 80-89.
[17] X. Xu, Y. Zhou, M. Fan, Z. Lv, Y. Tang, Y. Sun, Y. Chen, P. Wan, Lithium adsorption performance of a three-dimensional porous H2TiO3-type lithium ion-sieve in strong alkaline Bayer liquor, RSC Advances, 7 (2017) 18883-18891.
[18] D. Liu, Z. Zhao, W. Xu, J. Xiong, L. He, A closed-loop process for selective lithium recovery from brines via electrochemical and precipitation, Desalination, 519 (2021).
[19] B. Swain, Separation and purification of lithium by solvent extraction and supported liquid membrane, analysis of their mechanism: a review, Journal of Chemical Technology & Biotechnology, 91 (2016) 2549-2562.
[20] W. Xu, L. He, Z. Zhao, Lithium extraction from high Mg/Li brine via electrochemical intercalation/de-intercalation system using LiMn2O4 materials, Desalination, 503 (2021).
[21] S. Gmar, A. Chagnes, Recent advances on electrodialysis for the recovery of lithium from primary and secondary resources, Hydrometallurgy, 189 (2019) 105124.
[22] M.S. Palagonia, D. Brogioli, F. La Mantia, Lithium recovery from diluted brine by means of electrochemical ion exchange in a flow-through-electrodes cell, Desalination, 475 (2020).
[23] X. Zhao, H. Yang, Y. Wang, Z. Sha, Review on the electrochemical extraction of lithium from seawater/brine, J. Electroanal. Chem., 850 (2019) 113389.
[24] D. Gu, W. Sun, G. Han, Q. Cui, H. Wang, Lithium ion sieve synthesized via an improved solid state method and adsorption performance for West Taijinar Salt Lake brine, Chemical Engineering Journal, 350 (2018) 474-483.
[25] L. Zhang, D. Zhou, Q. Yao, J. Zhou, Preparation of H 2 TiO 3 -lithium adsorbent by the sol–gel process and its adsorption performance, Applied Surface Science, 368 (2016) 82-87.
[26] R.E.C. Torrejos, G.M. Nisola, H.S. Song, J.W. Han, C.P. Lawagon, J.G. Seo, S. Koo, H. Kim, W.-J. Chung, Liquid-liquid extraction of lithium using lipophilic dibenzo-14-crown-4 ether carboxylic acid in hydrophobic room temperature ionic liquid, Hydrometallurgy, 164 (2016) 362-371.
[27] X. Li, Y. Mo, W. Qing, S. Shao, C.Y. Tang, J. Li, Membrane-based technologies for lithium recovery from water lithium resources: A review, Journal of Membrane Science, 591 (2019) 117317.
[28] C.P. Lawagon, G.M. Nisola, J. Mun, A. Tron, R.E.C. Torrejos, J.G. Seo, H. Kim, W.-J. Chung, Adsorptive Li+ mining from liquid resources by H2TiO3: Equilibrium, kinetics, thermodynamics, and mechanisms, Journal of Industrial and Engineering Chemistry, 35 (2016) 347-356.
[29] H.-J. Hong, T. Ryu, I.-S. Park, M. Kim, J. Shin, B.-G. Kim, K.-S. Chung, Highly porous and surface-expanded spinel hydrogen manganese oxide (HMO)/Al2O3 composite for effective lithium (Li) recovery from seawater, Chemical Engineering Journal, 337 (2018) 455-461.
[30] S. Wang, X. Chen, Y. Zhang, Y. Zhang, S. Zheng, Lithium adsorption from brine by iron-doped titanium lithium ion sieves, Particuology, 41 (2018) 40-47.
[31] R. Chitrakar, Y. Makita, K. Ooi, A. Sonoda, Lithium recovery from salt lake brine by H2TiO3, Dalton Trans, 43 (2014) 8933-8939.
[32] F. Marchini, D. Rubi, M. del Pozo, F.J. Williams, E.J. Calvo, Surface Chemistry and Lithium-Ion Exchange in LiMn2O4 for the Electrochemical Selective Extraction of LiCl from Natural Salt Lake Brines, The Journal of Physical Chemistry C, 120 (2016) 15875-15883.
[33] R. Chitrakar, Y. Makita, K. Ooi, A. Sonoda, Selective Uptake of Lithium Ion from Brine by H1.33Mn1.67O4 and H1.6Mn1.6O4, Chemistry Letters, 41 (2012) 1647-1649.

[34] F. Qian, B. Zhao, M. Guo, Z. Wu, W. Zhou, Z. Liu, Surface trace doping of Na enhancing structure stability and adsorption properties of Li1.6Mn1.6O4 for Li+ recovery, Separation and Purification Technology, 256 (2021) 117583.
[35] J. Xiao, X. Nie, S. Sun, X. Song, P. Li, J. Yu, Lithium ion adsorption–desorption properties on spinel Li4Mn5O12 and pH-dependent ion-exchange model, Advanced Powder Technology, 26 (2015) 589-594.
[36] Z. Qiu, M. Wang, Y. Chen, T. Zhang, D. Yang, F. Qiu, Li4Mn5O12 doped cellulose acetate membrane with low Mn loss and high stability for enhancing lithium extraction from seawater, Desalination, 506 (2021).
[37] L.-Y. Zhang, Y.-W. Liu, L. Huang, N. Li, A novel study on preparation of H2TiO3–lithium adsorbent with titanyl sulfate as titanium source by inorganic precipitation–peptization method, RSC Advances, 8 (2018) 1385-1391.
[38] D. Tang, D. Zhou, J. Zhou, P. Zhang, L. Zhang, Y. Xia, Preparation of H2TiO3–lithium adsorbent using low-grade titanium slag, Hydrometallurgy, 157 (2015) 90-96.
[39] X.-c. Shi, Z.-b. Zhang, D.-f. Zhou, L.-f. Zhang, B.-z. Chen, L.-l. Yu, Synthesis of Li+ adsorbent (H2TiO3) and its adsorption properties, Transactions of Nonferrous Metals Society of China, 23 (2013) 253-259.
[40] F. Hayashi, K. Ogawa, Y. Moriya, T. Sudare, K. Teshima, Growth of β-Li2TiO3 Nanocrystals from LiCl and LiOH Fluxes, Crystal Growth & Design, 19 (2018) 1377-1383.
[41] A. Devie, M. Dubarry, H.-P. Wu, T.-H. Wu, B.Y. Liaw, Overcharge Study in Li4Ti5O12Based Lithium-Ion Pouch Cell, Journal of The Electrochemical Society, 163 (2016) A2611-A2617.
[42] S. Wang, P. Li, W. Cui, H. Zhang, H. Wang, S. Zheng, Y. Zhang, Hydrothermal synthesis of lithium-enriched β-Li2TiO3 with an ion-sieve application: excellent lithium adsorption, RSC Advances, 6 (2016) 102608-102616.
[43] L. Zhang, D. Zhou, G. He, F. Wang, J. Zhou, Effect of crystal phases of titanium dioxide on adsorption performance of H2TiO3-lithium adsorbent, Materials Letters, 135 (2014) 206-209.
[44] G. He, L. Zhang, D. Zhou, Y. Zou, F. Wang, The optimal condition for H2TiO3–lithium adsorbent preparation and Li+ adsorption confirmed by an orthogonal test design, Ionics, 21 (2015) 2219-2226.
[45] Z. Li-Yuan, X.-J. Wan, Y. Shui, Y.-H. You, Y.-W. Liu, S.-Q. Ruan, M. Su, The Effect of Surfactants on the Properties of Colloid Precursor Li2TiO3, Russian Journal of Physical Chemistry A, 94 (2020) 590-603.
[46] Y. Gan, J. Li, L. Zhang, B. Wu, W. Huang, H. Li, S. Zhang, Potential of titanium coagulants for water and wastewater treatment: Current status and future perspectives, Chemical Engineering Journal, 406 (2021).
[47] I. El Saliby, Y. Okour, H.K. Shon, J. Kandasamy, W.E. Lee, J.-H. Kim, TiO_2 nanoparticles and nanofibres from $TiCl_4$ flocculated sludge: Characterisation and photocatalytic activity, Journal of Industrial and Engineering Chemistry, 18 (2012) 1033-1038.
[48] Y. Okour, H.K. Shon, I.J. El Saliby, R. Naidu, J.B. Kim, J.H. Kim, Preparation and characterisation of titanium dioxide (TiO_2) and thiourea-doped titanate nanotubes prepared from wastewater flocculated sludge, Bioresour Technol, 101 (2010) 1453-1458.
[49] H.K. Shon, S. Vigneswaran, I.S. Kim, J. Cho, G.J. Kim, J.B. Kim, J.H. Kim, Preparation of titanium dioxide (TiO_2) from sludge produced by titanium tetrachloride ($TiCl_4$) flocculation of wastewater, Environ Sci Technol, 41 (2007) 1372-1377.
[50] B.C. Lee, S. Kim, H.K. Shon, S. Vigneswaran, S.D. Kim, J. Cho, I.S. Kim, K.H. Choi, J.B. Kim, H.J. Park, J.H. Kim, Aquatic toxicity evaluation of TiO2 nanoparticle produced from sludge of TiCl4 flocculation of wastewater and seawater, Journal of Nanoparticle Research, 11 (2008) 2087-2096.
[51] S.H. Na, H.K. Shon, J.B. Kim, H.J. Park, D.L. Cho, I.E. Saliby, J.H. Kim, Recycling of excess sludge using titanium tetrachloride ($TiCl_4$) as a flocculant aid with alkaline-thermal hydrolysis, Journal of Industrial and Engineering Chemistry, 16 (2010) 96-100.
[52] J.B. Kim, D.-H. Seol, H.K. Shon, G.-J. Kim, J.-H. Kim, Preparation and Characterization of Titania Nanoparticles from Titanium Tetrachloride and Titanium Sulfate Flocculation of Dye Wastewater, Journal of the Japan Petroleum Institute, 53 (2010) 167-172.

[53] I.J. El Saliby, H.K. Shon, Y.H. Okour, S. Vigneswaran, M. Senthilnanthanan, J. Kandasamy, Production of titanium dioxide nanoparticles and nanostructures from dye wastewater sludge - characterisation and evaluation of photocatalytic activity, Journal of Advanced Oxidation Technologies, 13 (2010) 15-20.
[54] Y.X. Zhao, B.Y. Gao, G.Z. Zhang, Q.B. Qi, Y. Wang, S. Phuntsho, J.H. Kim, H.K. Shon, Q.Y. Yue, Q. Li, Coagulation and sludge recovery using titanium tetrachloride as coagulant for real water treatment: A comparison against traditional aluminum and iron salts, Separation and Purification Technology, 130 (2014) 19-27.
[55] L. Zhao, Y. Liu, L. Wang, H. Zhao, D. Chen, B. Zhong, J. Wang, T. Qi, Production of Rutile TiO2 Pigment from Titanium Slag Obtained by Hydrochloric Acid Leaching of Vanadium-Bearing Titanomagnetite, Industrial & Engineering Chemistry Research, 53 (2013) 70-77.
[56] Y. Okour, H.K. Shon, H. Liu, J.B. Kim, J.H. Kim, Seasonal variation in the properties of titania photocatalysts produced from Ti-salt flocculated bioresource sludge, Bioresour Technol, 102 (2011) 5545-5549.
[57] J. Gong, J.C. Joo, J.K. Kim, Preparation and Characteristic Evaluation of Low-Cost TiO2 Photocatalyst, J Korean Soc Environ Eng, 41 (2019) 196-203.
[58] H.K. Shon, S. Vigneswaran, J. Kandasamy, M.H. Zareie, J.B. Kim, D.L. Cho, J.H. Kim, Preparation and characterization of titanium dioxide (TiO_2) from sludge produced by $TiCl_4$ flocculation with $FeCl_3$, $Al_2(SO_4)_3$ and $Ca(OH)_2$ coagulant aids in wastewater, Separation Science and Technology, 44 (2009) 1525-1543.
[59] S.M. Hossain, M.J. Park, H.J. Park, L. Tijing, J.H. Kim, H.K. Shon, Preparation and characterization of TiO2 generated from synthetic wastewater using TiCl4 based coagulation/flocculation aided with Ca(OH)2, J Environ Manage, 250 (2019) 109521.
[60] X. Li, L. Chen, Y. Chao, W. Chen, J. Luo, J. Xiong, F. Zhu, X. Chu, H. Li, W. Zhu, Amorphous TiO2 ‐ Derived Large ‐ Capacity Lithium Ion Sieve for Lithium Recovery, Chemical Engineering & Technology, 43 (2020) 1784-1791.
[61] K. Kataoka, Y. Takahashi, N. Kijima, H. Nagai, J. Akimoto, Y. Idemoto, K.-i. Ohshima, Crystal growth and structure refinement of monoclinic Li2TiO3, Materials Research Bulletin, 44 (2009) 168-172.
[62] C.P. Lawagon, G.M. Nisola, R.A.I. Cuevas, H. Kim, S.-P. Lee, W.-J. Chung, Development of high capacity Li+ adsorbents from H2TiO3/polymer nanofiber composites: Systematic polymer screening, characterization and evaluation, Journal of Industrial and Engineering Chemistry, 70 (2019) 124-135.
[63] L.A. Limjuco, G.M. Nisola, C.P. Lawagon, S.-P. Lee, J.G. Seo, H. Kim, W.-J. Chung, H 2 TiO 3 composite adsorbent foam for efficient and continuous recovery of Li + from liquid resources, Colloids and Surfaces A: Physicochemical and Engineering Aspects, 504 (2016) 267-279.
[64] S.M. Hossain, H. Park, H.J. Kang, J.S. Mun, L. Tijing, I. Rhee, J.H. Kim, Y.S. Jun, H.K. Shon, Facile synthesis and characterization of anatase TiO2/g-CN composites for enhanced photoactivity under UV-visible spectrum, Chemosphere, 262 (2021) 128004.
[65] S.M. Hossain, H. Park, H.-J. Kang, J.S. Mun, L. Tijing, I. Rhee, J.-H. Kim, Y.-S. Jun, H.K. Shon, Modified Hydrothermal Route for Synthesis of Photoactive Anatase TiO2/g-CN Nanotubes from Sludge Generated TiO2, Catalysts, 10 (2020).
[66] S.M. Hossain, H. Park, H.J. Kang, J.S. Mun, L. Tijing, I. Rhee, J.H. Kim, Y.S. Jun, H.K. Shon, Synthesis and NOx removal performance of anatase S-TiO2/g-CN heterojunction formed from dye wastewater sludge, Chemosphere, 275 (2021) 130020.
[67] L. Zhang, G. He, D. Zhou, J. Zhou, Q. Yao, Study on transformation mechanism of lithium titanate modified with hydrochloric acid, Ionics, 22 (2016) 2007-2014.
[68] C.L. Yu, F. Wang, S.Y. Cao, D.P. Gao, H.B. Hui, Y.Y. Guo, D.Y. Wang, The structure of H2TiO3-a short discussion on "Lithium recovery from salt lake brine by H2TiO3", Dalton Trans, 44 (2015) 15721-15724.
[69] C.-L. Yu, K. Yanagisawa, S. Kamiya, T. Kozawa, T. Ueda, Monoclinic Li2TiO3 nano-particles via hydrothermal reaction: Processing and structure, Ceramics International, 40 (2014) 1901-1908.
[70] F. Tielens, M. Calatayud, A. Beltrán, C. Minot, J. Andrés, Lithium insertion and mobility in the TiO2-anatase/titanate structure: A periodic DFT study, J. Electroanal. Chem., 581 (2005) 216-223.

[71] M. Thommes, K. Kaneko, A.V. Neimark, J.P. Olivier, F. Rodriguez-Reinoso, J. Rouquerol, K.S.W. Sing, Physisorption of gases, with special reference to the evaluation of surface area and pore size distribution (IUPAC Technical Report), Pure and Applied Chemistry, 87 (2015) 1051-1069.
[72] S.M. Hossain, L. Tijing, N. Suzuki, A. Fujishima, J.-H. Kim, H.K. Shon, Visible light activation of photocatalysts formed from the heterojunction of sludge-generated TiO2 and g-CN towards NO removal, Journal of Hazardous Materials, 422 (2022).
[73] Y. Jang, E. Chung, Adsorption of Lithium from Shale Gas Produced Water Using Titanium Based Adsorbent, Industrial & Engineering Chemistry Research, 57 (2018) 8381-8387.
[74] H. Qiu, L. Lv, B.-c. Pan, Q.-j. Zhang, W.-m. Zhang, Q.-x. Zhang, Critical review in adsorption kinetic models, Journal of Zhejiang University-SCIENCE A, 10 (2009) 716-724.
[75] S. Wang, M. Zhang, Y. Zhang, Y. Zhang, S. Qiao, S. Zheng, High adsorption performance of the Mo-doped titanium oxide sieve for lithium ions, Hydrometallurgy, 187 (2019) 30-37.
[76] M. Mohammad, M. Lisiecki, K. Liang, A. Razmjou, V. Chen, Metal-Phenolic network and metal-organic framework composite membrane for lithium ion extraction, Applied Materials Today, 21 (2020).